Co-Expression of Type 1 Fimbriae and Flagella in *Escherichia coli*: Consequences for Adhesion at Interfaces

Udayanidhi Ramesh Kumar, Nam T. Nguyen, Narendra K. Dewangan, Sayed Golam Mohiuddin, Mehmet A. Orman, Patrick C. Cirino*, and Jacinta C. Conrad*

*Corresponding authors
Department of Chemical and Biomolecular Engineering, University of Houston, Houston, TX 77204, USA
E-mail: pccirino@uh.edu, jcconrad@uh.edu

ABSTRACT

Escherichia coli expresses surface appendages including fimbriae, flagella, and curli, at various levels in response to environmental conditions and external stimuli. Previous studies have revealed an interplay between expression of fimbriae and flagella in several *E. coli* strains, but how this regulation between fimbrial and flagellar expression affects adhesion to interfaces is incompletely understood. Here, we investigate how the concurrent expression of fimbriae and flagella by engineered strains of *E. coli* MG1655 affects their adhesion at liquid-solid and liquid-liquid interfaces. We tune fimbrial and flagellar expression on the cell surface through plasmid-based inducible expression of the *fim* operon and *fliC-flhDC* genes. We show that increased fimbrial expression increases interfacial adhesion as well as bacteria-driven actuation of micron-sized objects. Co-expression of flagella in fimbriated bacteria, however, does not greatly affect either of these properties. Together, these results suggest that interfacial adhesion as well as motion actuated by adherent bacteria can be altered by controlling the expression of surface appendages.

INTRODUCTION

In nature, bacteria live and grow at liquid-liquid and solid-liquid interfaces,[1] forming surface-associated communities where they are able to attach. In practical applications, adhesion of bacteria at oil-liquid interfaces is reported to enhance the rate of biodegradation of hydrocarbons[2,3] and biofilms at solid-liquid interfaces can enhance the yield of value-added products in biochemical industries[4,5]. Finally, swimming bacteria can attach to objects in solution and shuttle them as cargo.[6,7] Thus, there is enduring interest in understanding the mechanisms used by bacteria for interfacial adhesion.

To adhere at interfaces, bacteria employ surface appendages including type 1 fimbriae,[8–14] flagella,[8,12,14–18] and curli,[19] as well as cell surface components such as Antigen 43 and other autotransporter proteins. Two of the best studied adhesins are type 1 fimbriae and

flagella. Type 1 fimbriae are 0.3 – 1.5 μm long and 7 nm wide thread-like structures that produce pN-scale forces to facilitate adhesion to solid surfaces and to liquid-liquid interfaces.[20] They also help bacteria evade antibiotics during initial infection and thus are an essential virulence factor of pathogenic bacteria.[21,22] Type 1 fimbriae are highly expressed during the biofilm formation and maturation, but not in the exponential and stationary phases of planktonic growth.[23] Flagella are 20 μm long and 20 – 40 nm wide filamentous structures that drive locomotion in motile bacteria.[24] In addition to imparting motility, flagella can also produce nN-scale forces that facilitate adhesion to surfaces.[17,25]

Type 1 fimbriae biosynthesis requires a large number of *fim* gene clusters belonging to the chaperone-usher assembly class, namely *fimB*, *fimE*, *fimA*, *fimI*, *fimC*, *fimD*, *fimF*, *fimG*, and *fimH*.[26,27] *fimA*, *fimF*, *fimG*, and *fimH* encode for the four protein components of type 1 fimbriae, with the main structural *fimA* subunit forming the helical rod, and *fimH* located at the fimbrial tip. *fimH* is connected to the rod through the *fimG* and *fimF* subunits, altogether forming the tip fibrillum. *fimC* is a periplasmic chaperone protein that mediates the assembly of type 1 fimbriae together with the outer membrane usher *fimD*. *fimB* and *fimE* encode regulatory proteins that control the type 1 fimbrial expression.[28,29] The genes responsible for flagellum synthesis, by contrast, form a highly regulated cascade of three classes. The class 1 master regulon *flhDC* encodes a transcription factor required for the transcription of class 2 genes that encode the basal body and hook of the flagellum, along with *fliA*. FliA is a sigma factor responsible for the transcription of the class 3 genes that encode hook-associated proteins, the filament of the flagellum (*fliC*), and other proteins necessary for motility and chemotaxis.[30] Since biosynthesis of fimbriae and flagella is energetically costly,[8,31] fimbrial and flagellar expression are tightly regulated in *E. coli*.[32] Although the adhesive properties of type 1 fimbriae and flagella have been extensively studied,[33–38] how the interplay between fimbrial and flagellin expression affects bacterial adhesion to interfaces remains incompletely

understood. Here, we examine how the simultaneous expression of fimbriae and flagella by *Escherichia coli* affects its adhesion at liquid-solid and liquid-liquid interfaces. A plasmid encoding inducible over-expression of the *fim* operon was transformed into a *fimA* mutant strain (MG1655Δ*fimA*). Since over-expression of type 1 fimbriae results in a significant decrease in cell motility, another plasmid containing the *fim* operon as well as *flhDC* and *fliC* genes was transformed into MG1655Δ*fimA*, which when induced was able to simultaneously produce both type 1 fimbriae and flagella. We quantify the effects of fimbriation and flagellation on biofilm formation, adhesion to oil droplets, and the motion of microscopic droplets driven by bacteria. We find that increased fimbrial expression improves the ability of bacteria to adhere to solid surfaces and oil-liquid interfaces and thereby enhances bacteria-driven actuation of microscale objects. Increased flagellar expression in highly fimbriated bacteria, however, does not significantly affect either adhesion at interfaces or bacteria-driven actuation. These results suggest that that the co-expression of flagella and fimbriae can offer improved function in biohybrid systems in which bacteria interact with nearby interfaces.

MATERIALS AND METHODS

Strains, plasmids, and growth conditions. Bacterial strains and plasmids used in this study are listed in **Table 1**. Details of strain and plasmid construction can be found in the Supplementary Information. For initial propagation, cells from 25% glycerol cell stock stored at -80°C were streaked onto Lysogeny Broth (LB) agar plates (containing 15 g L^{-1} agar (BD Chemicals), 5 g L^{-1} yeast extract (BD Chemicals), 10 g L^{-1} tryptone (BD Chemicals), and 5 g L^{-1} NaCl (VWR Chemicals)) with 50 μg mL^{-1} apramycin sulfate (Indofine Chemical Company) and incubated at 37 °C for 18 h. Liquid cultures grown overnight were obtained by inoculating a single colony from the agar plates into LB broth (containing 5 g L^{-1} yeast extract, 10 g L^{-1} tryptone, and 5 g L^{-1} NaCl) with 50 μg mL^{-1} apramycin sulfate and incubated in an orbital

incubator shaker (Barnstead Lab-Line) at 37 °C for 12 h with aeration (250 rpm). Subcultures were prepared by inoculating 300 μL of the overnight culture into 10 mL of LB broth with 50 μg mL^{-1} apramycin sulfate and grown to late exponential phase in an orbital incubator shaker at 37 °C with aeration (250 rpm).

	Relevant Genetics	**Source**
Strains		
MG1655	F^- λ^- *ilvG- rfb*-50 *rph*-1	CGSC# 8237
MG1655Δ*fimA*	MG1655, *fimA* deleted	This study
Plasmids[a]		
p(blank)	Lab plasmid pPCC2000, derived from pPCC1322.[39] No ORF downstream of P*tac*	This study
p(*fim*)	Lab plasmid pPCC1401. *fim* operon under the control of P*tac*	(38)
p(*fim-fliC-flhDC*)	Lab plasmid pPCC2208. *fim* operon, *fliC*, and *flhDC* operon under the control of P*tac*	This study

[a]All plasmids contain pBR322 origin, *lacI*, promoter P*tac*, *aac* (Apr^R)

Table 1 Bacterial strains and plasmids used in this study.

Atomic force microscopy (AFM). AFM was used to visually confirm the presence or absence of fimbriae. Freshly cleaved mica sheets (Electron Microscopy Sciences) were attached to AFM specimen discs using non-conductive double-sided adhesive tabs (Microscopy Solutions) and coated with 10 μL of 0.01% poly-L-lysine (Sigma Aldrich). Bacterial cultures were grown overnight from a single colony and subcultured the following morning, starting with an optical density at 600 nm (OD_{600}) of 0.1. The subcultures were induced with 10 μM of isopropyl β-d-1-thiogalactopyranoside (IPTG) (Fisher Bioreagents) at OD_{600} of 0.5. After 4 hours of induction, 1 mL of bacterial culture was centrifuged at 800 g for 10 min, the supernatant was discarded, and the cells were resuspended in sterile MilliQ water. The resuspended cells were diluted to an OD_{600} of 0.1 and added to the poly-L-lysine coated mica sheets glued on specimen discs. The samples were left to dry for 1 hour and then scanned

using a Bruker Multi-mode AFM by means of ScanAsyst Air tip (Bruker) in ScanAsyst Air mode.

Flow cytometry. Bacterial cultures were grown overnight from a single colony and subcultured the following morning (starting at an OD_{600} of 0.1). The subcultures were induced with 10 μM of IPTG at OD_{600} of 0.5. At 0, 1, 2, 4, 6, and 8 h after induction, cells were diluted 1:100 in 1 mL Phosphate Buffer Saline (PBS) in flow cytometry tubes (5 mL round bottom Falcon tubes (BD Biosciences), size: 12 × 75 mm) to achieve the desired cell density (~10^6 – 10^7 cells mL^{-1}) for flow cytometry analysis. The resulting cell suspensions were treated with 20 μM Propidium Iodide (PI) (Thermo Fisher Scientific) and 1 μM Redox Sensor Green (RSG) (Thermo Fisher Scientific) dyes. The samples were incubated in the dark at 37 °C for 15 min before analysis with a conventional bench-top flow cytometer (NovoCyte 3000RYB, ACEA Biosciences Inc.). For flow cytometry analysis, a slow sample flow rate (14 μL min^{-1}) was chosen to have a core diameter of 7.7 μm. The instrument has a constant sheath flow rate of 6.5 mL min^{-1}. The PI stain was excited at 561 nm wavelength and detected with a 615/20 nm bandpass filter; the RSG stain was excited at 488 nm wavelength and detected with a 530/30 nm bandpass filter. At least 30,000 events were recorded for each sample. NovoExpress software was used to collect the data. Dead cells, obtained by treating live cells with 70% v/v ethanol, were used as a positive control.

Preparation of glass capillaries for microscopy experiments. Thin rectangular borosilicate capillaries (Vitrocom, 0.1 mm height, 1 mm width, 50 mm length, 0.07 mm wall thickness) were used as sample chambers for imaging experiments. To minimize the adhesion of bacteria and prevent wetting of oil drops on the inner surface of the glass capillary, the capillaries were made hydrophilic by treatment with oxygen plasma (Harrick plasma cleaner PDC-32G) for 5 – 10 min. The plasma-treated capillaries were immediately filled with

suspensions of bacteria or emulsions/bacteria for imaging to minimize any change in surface hydrophilicity during the experiment.

Confocal microscopy and single-cell tracking. The swimming speed of bacteria was determined from tracking of single cells in microscopy movies. For these experiments, bacterial cultures were grown overnight from a single colony and subcultured the following morning (starting at an OD_{600} of 0.1). The subcultures were induced with 10 μM of IPTG at OD_{600} of 0.5. At 0, 1, 2, 4, 6, and 8 h after induction, the samples were diluted to an OD_{600} of 0.1 to enable individual swimming cells to be imaged using confocal microscopy. 1 mL of each diluted sample was stained with 5 μM of SYTO™ 9 Green Fluorescent Nucleic Acid Stain (Thermo Fisher Scientific). After incubating for 5 mins in dark, the stained cells were injected into plasma-cleaned glass capillaries and imaged using a TCS SP8 confocal inverted microscope (Leica Microsystems DMi8) equipped with a 63× oil immersion objective lens (N.A. 1.4). For each sample, five series of 300 images at least 50 μm away from the walls of the capillaries at different locations were acquired at a frame rate of 8 frame s^{-1}. Using TrackMate in Fiji (a distribution of ImageJ) software,[40] individual cells were identified, located, and linked to obtain cell trajectories, from which we calculated the instantaneous swimming speed $v = (x(t + \Delta t) - x(t))/\Delta t$, where $\Delta t = 0.125$ s.

Biofilm formation assay. The effect of fimbriation on the formation of bacterial biofilms on solid surfaces over time was assessed using a biofilm formation assay.[41] This assay measures the formation of biofilms on the wall and/or bottom of a microtiter plate over time, relative to the growth rate of the bacteria. Bacterial cultures were grown overnight from a single colony and subcultured the following morning (starting at an OD_{600} of 0.1). The subcultures were induced with 10 μM of IPTG at OD_{600} of 0.5. After mixing, aliquots of 200 μL of cell culture were injected into wells of a sterile 96-well microtiter plate (Nunc™ MicroWell™ Flat-Bottom Microplate, 400 μL per well, Thermo Fisher Scientific). The microtiter plate was then

statically incubated at 37°C for 0, 1, 2, 4, 6, and 8 hours. After incubation, the OD_{600} values of the cell cultures were measured to quantify relative cell growth, and the liquid was removed by inverting the plate. Each well was washed three times in MilliQ water to remove any cells that were not attached to the wells; subsequently, the remaining cells were stained by adding 300 µL 0.1% w/v crystal violet (CV) dye in MilliQ water for 15 min. After incubation, the wells were washed thrice in MilliQ water to rid the plate of excess dye, and dried for an hour, after which 300 µL of 80:20 v/v ethanol:acetone mixture was added to solubilize the CV-stained biofilm. Finally, 200 µL of the solubilized CV-stained biofilm was transferred to a clear-bottom 96-well plate and the absorbance was measured using a microplate reader (Onetech Medical Equipment Co. Ltd.) to quantify the level of biofilm formation.

Pendant drop tensiometry. Pendant drop tensiometry was used to determine the interfacial tension of bacteria-laden oil-water interfaces. For the interfacial tension measurements, cells were harvested at 0, 1, 2, 4, 6, and 8 h after induction and centrifuged at 800 g for 10 min. The supernatants were discarded, and the cells were resuspended in PBS buffer solution. The samples were normalized to an OD_{600} of 2. The interfacial tension between the bacterial suspension and hexadecane oil was measured by the pendant drop method[42,43] using a pendant drop goniometer (DataPhysics OCA15EC). Briefly, a pendant drop of a bacterial suspension was formed at the tip of a needle (Hamilton Company, 27 gauge) immersed in hexadecane oil. The profile of the droplet was imaged using a camera (uEye camera) and the interfacial tension was determined from the radius of curvature of the drop using the Young-Laplace equation.[42]

Brightfield droplet assay. For imaging experiments, cells were harvested at 0, 1, 2, 4, 6, and 8 h after induction. Emulsions of hexadecane in LB broth were made by shaking 20 µL of hexadecane (≥99%, Sigma-Aldrich) in 300 µL of LB broth. To these emulsions, 10 µL of FluoSpheres™ Sulfate-Modified Microspheres (0.04% v/v, 0.02–4.0 µm, Thermo Fisher

Scientific) were added and the suspension was shaken again. The FluoSphere particles were added to aid in determining the drop's angular position over time. Using this technique, we obtained drops of diameter 10 – 100 μm. Then, 200 μL of cell suspension (OD_{600} of 1) was added and shaken gently by hand. Finally, 6.7 μL of the emulsion-bacteria suspension was injected into a glass microfluidic channel and both ends of the channel were sealed with vacuum grease. We used a brightfield inverted microscope (Leica Microsystems DM4000) equipped with a 40× oil immersion objective lens (HCX PL APO, N.A. 1.25–0.75) to image rotating droplets. Images of droplets located at least 200 μm away from the side walls of the capillaries, to avoid any interference from the lateral walls, were acquired for up to ten minutes after injection to ensure that the capillary surface remained hydrophilic throughout the measurement. Images were captured at a rate of 5 frames s^{-1} using a digital camera (Olympus DP21). We tracked the positions of the FluoSphere particles attached to the droplet interface for analyzing the droplet rotation and determined the angular speed of individual droplets from the slope of total rotation as a function of time.

RESULTS AND DISCUSSION

To quantitatively assess the role of type 1 fimbriae in *E. coli* on interfacial adhesion, we initially constructed a fimbria-deficient *E. coli* mutant, MG1655Δ*fimA*, by deleting the *fimA* gene from the reference strain *E. coli* MG1655. MG1655Δ*fimA* was further transformed with a plasmid carrying the *fim* operon, whereby addition of IPTG induces expression of type 1 fimbriae (**Fig. 1**). Our earlier study[38] showed that the plasmid p(*fim*) is slightly leaky using gene expression measurements, but that the leaky expression did not notably affect metrics for phenotypic expression of fimbriae. We expected that induced expression of the *fim* operon in MG1655Δ*fimA*+p(*fim*) would reduce cell motility due to the inverse regulation of fimbriation and flagellin expression observed in several *E. coli* strains, including *E. coli* MG1655.[32] An earlier study examining the regulation between fimbrial and flagellin expression

at the level of transcription reported an 85–fold increase in the level of *fimA* transcripts and a 46–fold decrease in *fliC* transcripts in an *E. coli* mutant that constitutively expressed type 1 fimbriae, relative to a wild-type strain.[32] Additionally, the study concluded that the downregulation of *fliC* transcription due to the over-expression of fimbriae resulted in a decrease in flagellin expression, leading to a significant decrease in cell motility. To restore motility, we added to this *fim* expression plasmid inducible expression of *fliC* as well as the *flhDC* operon, encoding the master motility regulator (**Fig. 1**).

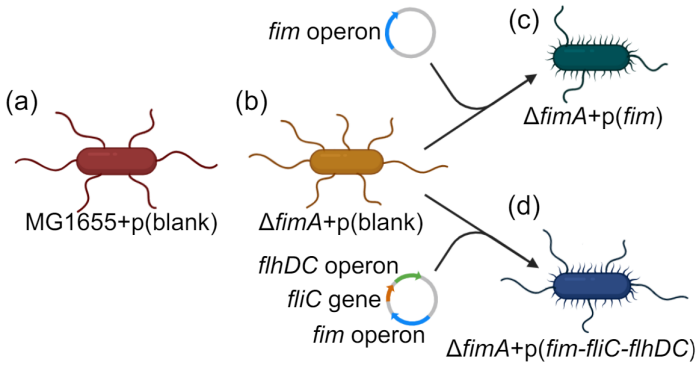

Fig. 1 Schematic of mutants used in this study: (a) *E. coli* MG1655+p(blank) strain, (b) the fimbrial deletion mutant MG1655Δ*fimA*+p(blank), (c) the engineered MG1655Δ*fimA*+p(*fim*), and (d) the engineered MG1655Δ*fimA*+p(*fim-fliC-flhDC*) strain.

The biosynthesis and assembly of fimbriae consume significant energy and carbon.[44] As a result, inducing extremely high expression of fimbriae may affect cell viability. We measured the effects of fimbrial expression level on cell viability by staining with Propidium Iodide (PI) and Redox Sensor Green (RSG) dye. PI is a red fluorescent dye that does not penetrate live cells, and thus is commonly used to detect dead cells in a population.[45] Penetration of PI through the cell membrane yields high PI fluorescence, indicating that the cell is dead or membrane compromised. RSG dye penetrates the cell membrane and acts as a fluorogenic indicator of cellular redox potential and hence metabolic activity.[46] Low RSG fluorescence implies that the cell has reduced metabolic activity. Thus, the combination of high PI fluorescence coupled with low RSG fluorescence identifies those cells that are dead with compromised membrane activity due to fimbrial expression.

We exposed *E. coli* MG1655, MG1655Δ*fimA*, and type 1 fimbriated MG1655Δ*fimA*+p(*fim*) and MG1655Δ*fimA*+p(*fim-fliC-flhDC*) cells induced with IPTG at various concentrations to PI and RSG and examined the fluorescence signals using flow cytometry. To determine the cutoffs for the fluorescence signal levels that indicated dead and membrane-compromised cells, we carried out a positive control experiment on cells treated with 70% v/v ethanol (**Fig. S1**). For both MG1655 and MG1655Δ*fimA* strains, fewer than 1% of cells are non-viable (i.e., dead or membrane-compromised) when grown in the presence of 10 μM or 100 μM IPTG. Meanwhile, 37% of MG1655Δ*fimA*+p(*fim*) cells and 31% of MG1655Δ*fimA*+p(*fim-fliC-flhDC*) cells are non-viable when grown in the presence of 100 μM IPTG (**Fig. 2**). By contrast, fewer than 4% of MG1655Δ*fimA*+p(*fim*) and MG1655Δ*fimA*+p(*fim-fliC-flhDC*) cells lose their viability when grown with 10 μM IPTG (**Fig. 2**). Therefore, we used 10 μM as the concentration to induce fimbrial expression in all future experiments. We note that some fimbriated cells had both high PI and high RSG fluorescence. We posit that these cells may express more fimbriae, leading to more pore formation on their cell surfaces and high PI fluorescence, but not to the extent of compromising their viability and membrane integrity, resulting in high RSG fluorescence.

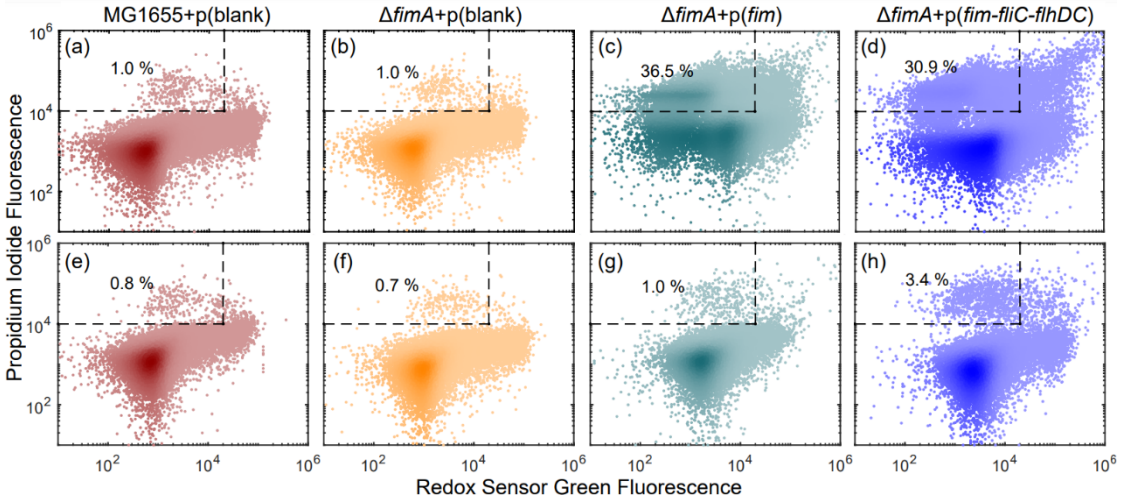

Fig. 2 PI and RSG staining to determine the cell viability for the choice of optimum IPTG concentration (a -- d) 100 μM and (e -- h) 10 μM. *E. coli* (a) MG1655+p(blank) cells, (b) fimbriae deleted cells MG1655Δ*fimA*+p(blank), and type 1 fimbriated (c) MG1655Δ*fimA*+p(*fim*) and (d) MG1655Δ*fimA*+p(*fim-fliC-flhDC*) cells grown in the presence of 100 μM IPTG for 4 h; (e) MG1655 cells, (f) MG1655Δ*fimA*, and (g) MG1655Δ*fimA*+p(*fim*)

and (h) MG1655Δ*fimA*+p(*fim-fliC-flhDC*) cells grown in the presence of 10 μM IPTG for 4 h were stained with PI and RSG dye and analyzed by flow cytometry. Cell viability is significantly affected by fimbrial expression induced with 100 μM IPTG, but not with 10 μM IPTG. The horizontal and vertical dashed lines indicate the gating cutoffs for the PI and RSG fluorescence, respectively. The percentage values are the percentage of dead and membrane-compromised cells in the cell population. A representative replicate is shown, but similar data were obtained for three biological replicates.

To confirm that strains engineered for fimbriae expression produced fimbriae, we imaged cells using atomic force microscopy. The MG1655Δ*fimA*+p(*fim*) and MG1655Δ*fimA*+p(*fim-fliC-flhDC*) strains produce fimbriae when induced with 10 μm IPTG, whereas neither MG1655 nor MG1655Δ*fimA* express any fimbriae upon induction (**Fig. 3**). AFM imaging also revealed that the strains express different numbers of flagella. Both MG1655 and MG1655Δ*fimA* express 3 to 6 flagella per cell. This result is consistent with an earlier study that showed loss of fimbrial production in *E. coli* MG1655 does not affect flagellation.[32] The MG1655Δ*fimA*+p(*fim*) strain, however, expresses fewer flagella (2 to 4 per cell) than the reference strain (Figure S2). We attribute this reduction in flagellar expression to the inverse regulatory relationship between fimbrial and flagellin expression previously studied in this strain.[32] Finally, the MG1655Δ*fimA*+p(*fim-fliC-flhDC*) strain expresses the same number of flagella as MG1655 (3 to 6 per cell) as a result of induced *flhDC* expression. These results confirm that we can control fimbrial and flagellar expression on the cell surface through induction of *fim* and *flhDC* operons.

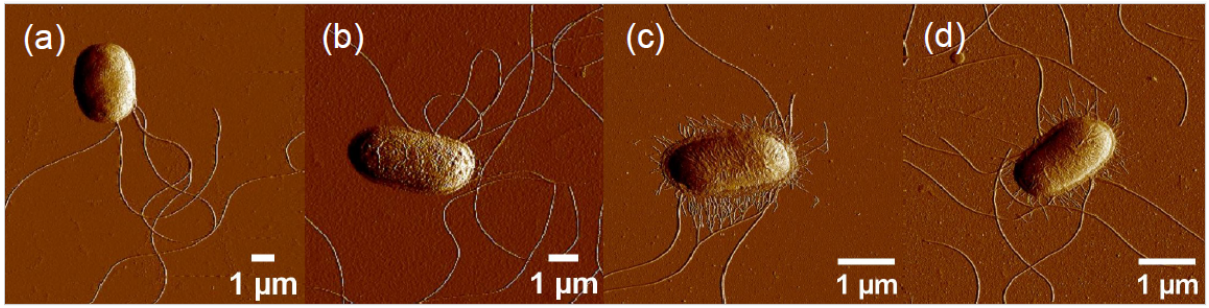

Fig. 3 Representative AFM images of (a) the MG1655+p(blank) strain, (b) the fimbrial deletion mutant MG1655Δ*fimA*+p(blank), (c) the induced engineered MG1655Δ*fimA*+p(*fim*), and (d) the induced engineered MG1655Δ*fimA*+p(*fim-fim-flhDC*) strain. All strains were grown in the presence of 10 μM IPTG for 4 h.

To study the effect of fimbriation on cell motility, we measured the instantaneous swimming speed of individual bacterial cells using confocal microscopy and single cell tracking algorithms. The distribution of the swimming speeds of individual cells does not follow a Gaussian distribution (**Fig. 4**). Thus, we were unable to identify an appropriate statistical distribution that could model all of our data. For statistical comparison we therefore selected CDF = 0.5 (that is, the speed of the median cell in the population) to compare across the different strains. The swimming speeds at which CDF = 0.5 for the MG1655, MG1655Δ*fimA*, MG1655Δ*fimA*+p(*fim*), and MG1655Δ*fimA*+p(*fim-fliC-flhDC*) strains are 8±2 μm s^{-1}, 8±1 μm s^{-1}, 2±0 μm s^{-1}, and 6±1 μm s^{-1}, respectively. Thus, the reference MG1655 and MG1655Δ*fimA* strains have the fastest swimming speed. Removal of type 1 fimbriae does not affect cell motility, whereas induction of fimbrial expression reduces motility, as also shown in an earlier study.[32] Induction of *flhDC* expression concurrent with *fim* expression, however, nearly restores the motility decreased by fimbrial expression.

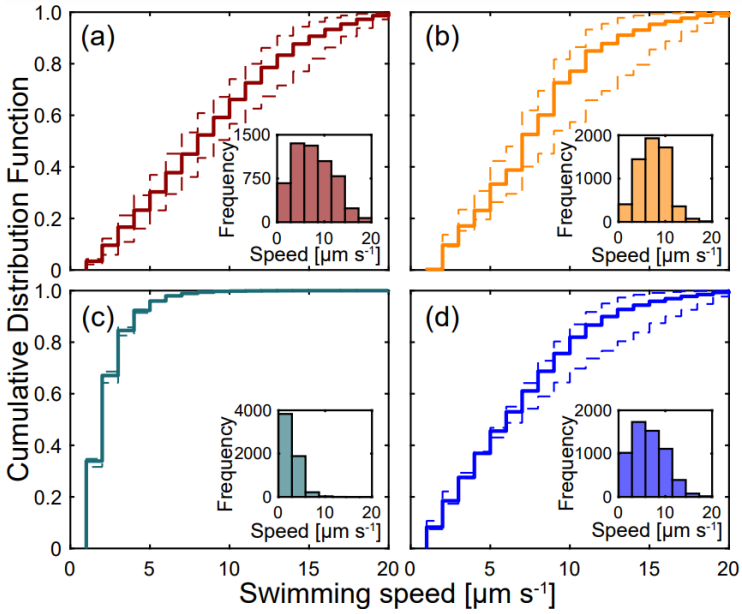

Fig. 4 The cumulative distribution function of instantaneous swimming speeds of different strains: (a) MG1655+p(blank) + 10 μM IPTG; (b) MG1655Δ*fimA*+p(blank) + 10 μM IPTG; (c) MG1655Δ*fimA*+p(*fim*) + 10 μM IPTG; (d) MG1655Δ*fimA*+p(*fim-fliC-flhDC*) + 10 μM IPTG at 4 h after induction. The inset depicts the histogram of the instantaneous swimming speed of the corresponding bacterial strain. Expression of fimbriae reduces cell motility. Induction of *flhDC* expression partially restores the reduced motility. Three biological replicates were measured to plot the cumulative distribution function of instantaneous swimming speeds of each strain. Dashed lines represent 95% confidence intervals. A histogram

of the instantaneous swimming speed is shown for a representative replicate of each strain, but similar data were obtained for three biological replicates.

We tested the ability of the strains engineered for fimbriae expression to adhere to and produce biofilm on solid surfaces using a Crystal Violet (CV) assay.[41] The measured absorbance of the CV-stained biofilm per cell density correlates with the amount of biofilm formation. The fimbriated MG1655Δ*fimA*+p(*fim*) and MG1655Δ*fimA*+p(*fim-fliC-flhDC*) strains form more biofilm than MG1655 and MG1655Δ*fimA*, neither of which express fimbriae (**Fig. 5**). The absorbance level of CV-stained biofilm per cell density for the MG1655 and MG1655Δ*fimA* strains is negligible until 8 h after induction and does not increase with respect to the time after induction. By contrast, the amount of biofilm produced by the fimbriated MG1655Δ*fimA*+p(*fim*) and MG1655Δ*fimA*+p(*fim-fliC-flhDC*) strains increases with the time after induction (**Fig. 5**). This result confirms that type 1 fimbriae promote biofilm formation in *E. coli,* consistent with prior studies.[8,23,47] Flagellar expression in MG1655Δ*fimA*+p(*fim-fliC-flhDC*), however, does not lead to significantly more biofilm than in the MG1655Δ*fimA*+p(*fim*) strain. In the MG1655Δ*fimA*+p(*fim-fliC-flhDC*) strain, biofilm growth is not statistically different between 6 and 8 h. We speculate that the slight decrease after 6 h may be due to nutrient deprivation, because this strain uses more energy by co-expressing fimbriae and flagella.

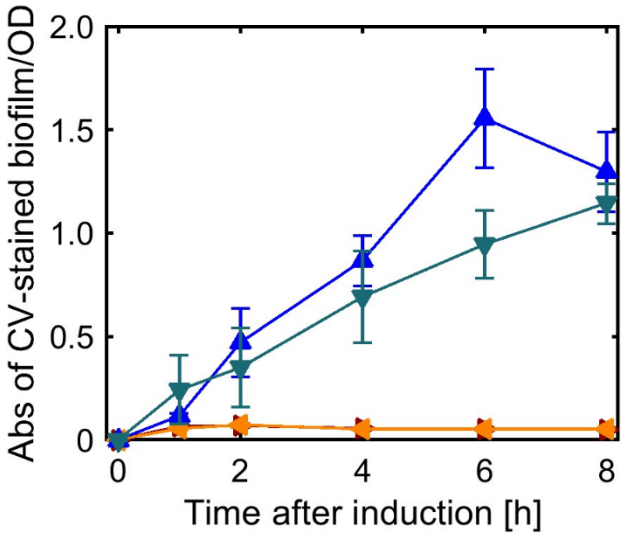

Fig. 5 Quantification of biofilm formation as a function of time after induction for different strains. The MG1655Δ*fimA*+p(*fim*) and MG1655Δ*fimA*+p(*fim-fliC-flhDC*) strains form more biofilm than MG1655 and MG1655Δ*fimA*. Symbols: (►) MG1655+p(blank) + 10 μM IPTG; (◄) MG1655Δ*fimA*+p(blank) + 10 μM IPTG; (▼) MG1655Δ*fimA*+p(*fim*) + 10 μM IPTG; (▲) MG1655Δ*fimA*+p(*fim-fliC-flhDC*) + 10 μM IPTG. Three biological replicates were measured for each sample. Error bars represent standard deviations.

We tested the ability of the strains engineered for fimbriae expression to adhere to the liquid-hexadecane interface using the pendant drop method for measuring interfacial tension.[48] The interfacial tension of the liquid-hexadecane interface decreased by ~5 mN m^{-1} when MG1655 cells are added to the liquid phase (**Table 2**).[48] The interfacial tensions of the oil-water interface in the presence of MG1655 and MG1655Δ*fimA* are not significantly different (**Table 2**). In the presence of a strain expressing fimbriae (MG1655Δ*fimA*+p(*fim*) or MG1655Δ*fimA*+p(*fim-fliC-flhDC*)), however, the interfacial tension decreases more (~7.5 mN m^{-1}) than compared to addition of fimbriae-deficient cells (**Table 2**). This result implies that fimbrial expression enhances the ability of bacteria to stick to liquid-oil interfaces, which is consistent with previous studies[23,38] in which a MATH (Microbial Adhesion To Hydrocarbons) assay was used to semi-quantitatively assess bacterial adhesion to oil–liquid interfaces. Co-expression of flagella does not significantly alter the interfacial tension, however, indicating that flagella do not strongly affect the ability of highly fimbriated bacteria to adhere to liquid-liquid interfaces.

Strains	**Interfacial tension [mN m^{-1}]**
No cells (Control)	51.5±0.8
MG1655+p(blank)	46.5±0.5
MG1655Δ*fimA*+p(blank)	47.4±1.5
MG1655Δ*fimA*+p(*fim*)	44.1±0.9
MG1655Δ*fimA*+p(*fim-fliC-flhDC*)	44.3±0.8

Table 2 Measurement of interfacial tension of the bacteria-hexadecane interface for different strains induced with 10 μM IPTG for 4 h. The fimbriated MG1655Δ*fimA*+p(*fim*) and MG1655Δ*fimA*+p(*fim-fliC-flhDC*) strains significantly reduce the bacteria-oil interfacial tension more than the MG1655 and MG1655Δ*fimA* strains ($p < 0.05$). Measurements were made using bacterial cultures with $OD_{600} = 2$. Three biological replicates were measured for each sample.

Finally, we examined the effects of fimbriation on the ability of bacteria to actuate microscale motion by rotating a droplet of hexadecane, as in our previous study.[49] The rotation rate of droplets of ~25 μm diameter increases in the order MG1655 ≈ MG1655Δ*fimA* < MG1655Δ*fimA*+p(*fim*) ≈ MG1655Δ*fimA*+p(*fim-fliC-flhDC*) (**Table 3**). We attribute the differences in the rotation rate to differences in the ability of the bacteria to adhere to the oil-water interface. The MG1655+p(blank) and MG1655Δ*fimA*+p(blank) cells rotate droplets at a speed of 0.2 rpm (**Table 3**), consistent with the results of our previous study.[49] These bacteria are motile, confirmed by instantaneous swimming speed measurements (**Fig. 4**), but adhere less to the oil-liquid interface, as indicated by the interfacial tension measurements (**Table 2**). By contrast, the fimbriated MG1655Δ*fimA*+p(*fim*) and MG1655Δ*fimA*+p(*fim-fliC-flhDC*) cells adhere more strongly to the oil-liquid interface and can rotate hexadecane droplets at a higher speed of ~0.5 rpm. Notably, the rotation speed of hexadecane droplets driven by fimbriated MG1655Δ*fimA*+p(*fim*) and MG1655Δ*fimA*+p(*fim-fliC-flhDC*) cells are not significantly different even though these two strains bear different numbers of flagella (**Fig. 3**) and swim at different rates (**Fig. 4**). This comparison suggests that the difference in rotation rate is not due to flagella-driven adhesion or swimming but instead reflects the ability of bacteria to adhere at the liquid-oil interface, which is predominantly controlled by fimbriation. This conclusion is consistent with the findings of our earlier study of bacteria-driven droplet rotation, in which we compared the rotation rates for three species of bacteria (*E. coli*, *Shewanella haliotis*, and *Halomonas titanicae*).[49] In that study, all three species swam at similar speeds near surfaces but rotated droplets at different rates; the fastest rotation was observed for *H. titanicae*, which had the greatest number of cells adhered at the oil-water interface. Although fimbriated bacteria decrease the oil-water interfacial tension more than non-fimbriated bacteria (Table 2), the expression for the rotation rate of a bacteria-driven droplet obtained in our earlier study[49] does not include the interfacial tension. Thus, it is likely that fimbriation affects rotation by

increasing the number of adherent cells (which increases the torque from the bacteria) rather than by lowering the interfacial tension.

Strains	Angular speed (rpm)
MG1655+p(blank)	0.2±0.1
MG1655Δ*fimA*+p(blank)	0.2±0.1
MG1655Δ*fimA*+p(*fim*)	0.5±0.1
MG1655Δ*fimA*+p(*fim-fliC-flhDC*)	0.5±0.2

Table 3 Angular speed of hexadecane droplets of 25 μm diameter driven by different strains induced with 10 μM IPTG for 4 h. The fimbriated MG1655Δ*fimA*+p(*fim*) and MG1655Δ*fimA*+p(*fim-fliC-flhDC*) strains rotate hexadecane droplets suspended near solid surfaces at a higher speed than the MG1655+p(blank) and MG1655Δ*fimA*+p(blank) strains. Three biological replicates were measured for each sample and ~12 hexadecane droplets were analyzed for each condition.

CONCLUSION

We examined the effects of fimbrial and flagellar expression on biofilm formation, adhesion to oil droplets, and the motion of microscopic objects driven by bacteria. The MG1655Δ*fimA*+p(*fim*) and MG1655Δ*fimA*+p(*fim-fliC-flhDC*) strains express fimbriae when induced with 10 μm IPTG without significantly affecting their cell viability. The swimming speed of the MG1655Δ*fimA*+p(*fim*) strain is lower than that of the reference MG1655+p(blank) and fimbriae-deficient MG1655Δ*fimA*+p(blank) strains due to the reduced expression of flagella upon fimbriation, whereas induction of *flhDC* expression partially restores the reduced motility in the MG1655Δ*fimA*+p(*fim-fliC-flhDC*) strain. The MG1655Δ*fimA*+p(*fim*) and MG1655Δ*fimA*+p(*fim-fliC-flhDC*) strains adhere more to solid surfaces and oil-liquid interfaces and rotate hexadecane droplets suspended near solid surfaces at a higher speed than either the MG1655+p(blank) or MG1655Δ*fimA*+p(blank) strains. Intriguingly, co-expression of flagella in fimbriated bacteria does not appear to strongly affect biofilm formation (a proxy for adhesion at solid-liquid interfaces) or liquid-hexadecane interfacial tension (a proxy for adhesion at liquid-liquid interfaces). Similarly, the swimming speed and number of flagella do

not appear to strongly affect the droplet rotation rate. These results show that modulating the expression of surface structures can alter adhesion, which in turn can promote motion actuated by adherent bacteria. In future work, it may be interesting to whether other host strains (e.g., MG1655 or MG1655Δ*flhDC*) affect the phenotypic co-expression of fimbriae and flagella. More broadly, genetically modified bacteria such as ours, featuring tunable co-expression of fimbriae and flagella, may have applications in biohybrid active matter[50,51] as well as in targeted delivery of drugs[52–54] or self-healing materials.[55] More broadly, the approaches in this study enable quantitative physical studies using bacteria as tunable, living colloids to alter interfacial properties.

ACKNOWLEDGEMENTS

We acknowledge support from the National Science Foundation (DMR-2104796, to JCC and PCC) and the Welch Foundation (E-1869, to JCC). We thank Prof. Peter G. Vekilov (UH) for access to Atomic Force Microscopy.

CONFLICTS OF INTEREST

There are no conflicts of interest to declare.

ELECTRONIC SUPPLEMENTARY INFORMATION

The ESI contains information on strain and plasmid construction; Tables S1 (primers used in this study), S2 (number of CFU per mL at OD600 = 1) and S3 (comparison of significance values for interfacial tension measurements); and Figures S1 (flow cytometry control experiments), S2 (average number of flagella per cell), S3 (images of pendant drops), S4 (biofilm assay for uninduced strains), S5 (flow cytometry over time), S6 (swimming speeds

over time), S7 (interfacial tension over time), and S8 (angular speed of droplet rotation over time); and Supplementary Movies S1 – S4 (rotation of oil droplets).

REFERENCES

1. H. M. Lappin-Scott and J. William Costerton, *Biofouling*, 1989, **1**, 323–342.
2. H. Abbasnezhad, M. Gray and J. M. Foght, *Appl. Microbiol. Biotechnol.*, 2011, **92**, 653–675.
3. H. Abbasnezhad, J. M. Foght and M. R. Gray, *Biodegradation*, 2011, **22**, 485–496.
4. A. N. Tsoligkas, M. Winn, J. Bowen, T. W. Overton, M. J. H. Simmons and R. J. M. Goss, *ChemBioChem*, 2011, **12**, 1391–1395.
5. L. Cuny, D. Pfaff, J. Luther, F. Ranzinger, P. Ödman, J. Gescher, G. Guthausen, H. Horn and A. Hille-Reichel, *Biotechnol. Bioeng.*, 2019, **116**, 2687–2697.
6. L. Vaccari, M. Molaei, R. L. Leheny and K. J. Stebe, *Soft Matter*, 2018, **14**, 5643–5653.
7. D. B. Weibel, P. Garstecki, D. Ryan, W. R. DiLuzio, M. Mayer, J. E. Seto and G. M. Whitesides, *Proc. Natl. Acad. Sci. U. S. A.*, 2005, **102**, 11963–11967.
8. L. A. Pratt and R. Kolter, *Mol. Microbiol.*, 1998, **30**, 285–293.
9. V. Hancock, I. L. Witsø and P. Klemm, *Int. J. Med. Microbiol.*, 2011, **301**, 570–576.
10. O. Mol and B. Oudega, *FEMS Microbiol. Rev.*, 1996, **19**, 25–52.
11. X. Jin and J. S. Marshall, *PLoS One*, 2020, **15**, e0243280.
12. C. Berne, C. K. Ellison, A. Ducret and Y. V. Brun, *Nat. Rev. Microbiol.*, 2018, **16**, 616–627.
13. T. Proft and E. N. Baker, *Cell. Mol. Life Sci.*, 2009, **66**, 613–635.
14. T. E. P. Kimkes and M. Heinemann, *FEMS Microbiol. Rev.*, 2019, **44**, 106–122.
15. K. P. Lemon, D. E. Higgins and R. Kolter, *J. Bacteriol.*, 2007, **189**, 4418–4424.
16. J. Bruzaud, J. Tarrade, A. Coudreuse, A. Canette, J. M. Herry, E. Taffin de Givenchy, T. Darmanin, F. Guittard, M. Guilbaud and M. N. Bellon-Fontaine, *Colloids Surf B Biointerfaces*, 2015, **131**, 59–66.
17. R. S. Friedlander, N. Vogel and J. Aizenberg, *Langmuir*, 2015, **31**, 6137–6144.
18. R. Van Houdt and C. W. Michiels, *Res. Microbiol.*, 2005, **156**, 626–633.
19. D. M. Pawar, M. L. Rossman, J. Chen and J. Chen, *J. Appl. Microbiol.*, 2005, **99**, 418–425.
20. L. De La Fuente, E. Montanes, Y. Meng, Y. Li, T. J. Burr, H. C. Hoch and M. Wu, *Appl. Environ. Microbiol.*, 2007, **73**, 2690–2696.
21. I. Avalos Vizcarra, V. Hosseini, P. Kollmannsberger, S. Meier, S. S. Weber, M. Arnoldini, M. Ackermann and V. Vogel, *Sci. Rep.*, 2016, **6**, 18109.
22. H. Connell, W. Agace, P. Klemm, M. Schembri, S. Marild and C. Svanborg, *Proc. Natl. Acad. Sci. U. S. A.*, 1996, **93**, 9827-9832.
23. D. F. Rodrigues and M. Elimelech, *Biofouling*, 2009, **25**, 401–411.
24. H. Terashima, S. Kojima and M. Homma. *Int. Rev. Cell. Mol. Biol.*, 2008, **270**, 39– 85.
25. Y. Kovalenko, I. Sotiri, J. V. I. Timonen, J. C. Overton, G. Holmes, J. Aizenberg and C. Howell, *Adv. Healthc. Mater.*, 2017, **6**, 1600948.
26. P. Klemm, *Rev. Infect. Dis.*, 1985, **7**, 321–340.
27. S. D. Knight and J. Bouckaert *Top. Curr. Chem.*, 2009, **288**, 67–107.
28. D.L. Gally, J. Leathart and I.C. Blomfield, *Mol. Microbiol.*, 1996, **21**, 725–738.
29. P. Klemm, *EMBO J.*,1986, **5**, 1389–1393.

30. F. C. Neidhardt and R. Curtiss, *Escherichia Coli and Salmonella: Cellular and Molecular Biology*. Washington, D.C.: ASM Press, 1996.
31. O. A. Soutourina and P. N. Bertin, *FEMS Microbiol. Rev.*, 2003, **27**, 505–523.
32. M. C. Lane, A. N. Simms and H. L. T. Mobley, *J. Bacteriol.*, 2007, **189**, 5523–5533.
33. W. E. Thomas, L. M. Nilsson, M. Forero, E. V. Sokurenko and V. Vogel, *Mol. Microbiol.*, 2004, **53**, 1545–1557.
34. R. S. Friedlander, N. Vogel and J. Aizenberg, *Langmuir*, 2015, **31**, 6137–6144.
35. S. Sharma, Y. A. Jaimes-Lizcano, R. B. McLay, P. C. Cirino and J. C. Conrad, *Langmuir*, 2016, **32**, 5422–5433.
36. R. S. Friedlander, H. Vlamakis, P. Kim, M. Khan, R. Kolter and J. Aizenberg, *Proc. Natl. Acad. Sci. U. S. A.*, 2013, **110**, 5624–5629.
37. A. Persat, C. D. Nadell, M. K. Kim, F. Ingremeau, A. Siryaporn, K. Drescher, N. S. Wingreen, B. L. Bassler, Z. Gitai and H. A. Stone, *Cell*, 2015, **161**, 988–997.
38. R. B. McLay, H. N. Nguyen, Y. A. Jaimes-Lizcano, N. K. Dewangan, S. Alexandrova, D. F. Rodrigues, P. C. Cirino and J. C. Conrad, *Langmuir*, 2018, **34**, 1133–1142.
39. Z. Wang, A. Doshi, R. Chowdhury, Y. Wang, C. D. Maranas and P. C. Cirino, *Protein Eng. Des. Sel.* 2020, **33**, gzaa027.
40. J. E. Schindelin, I. Arganda-Carreras, E. Frise, V. Kaynig, M. Longair, T. Pietzsch, S. Preibisch, C. T. Rueden, S. Saalfeld, B. Schmid, J. Tinevez, D. J. White, V. Hartenstein, K. W. Eliceiri, P. Tomančák and A. Cardona, *Nat. Methods*, 2012, **9**, 676-682.
41. G. A. O'Toole, *J. Vis. Exp.*, 2011, **40**, 2437.
42. J. D. Berry, M. J. Neeson, R. R. Dagastine, D. Y. C. Chan and R. F. Tabor, *J. Colloid Interface Sci.*, 2015, **454**, 226–237.
43. N. K. Dewangan and J. C. Conrad, *Langmuir*, 2018, **34**, 14012–14021.
44. J. Qiao, X. Tan, H. Ren, Z. Wu, X. Hu and X. Wang, *Appl. Environ. Microbiol.,* 2021, **87**, e0038121.
45. L. Boulos, M. Prévost, B. Barbeau, J. Coallier and R. Desjardins, *J. Microbiol. Methods,* 1999, **37**, 77–86.
46. D. Gray, R. S. Yue, C. Y. Chueng and W. Godfrey, *105th Gen. Meet. Am. Soc. Microbiol.,* 2005, 331.
47. C. Blumer, A. Kleefeld, D. Lehnen, M. Heintz, U. Dobrindt, G. Nagy, K. Michaelis, L. Emödy, T. Polen, R. Rachel, V. F. Wendisch and G. Unden, *Microbiology (Reading)*, 2005, **151**, 3287–329
48. N. S. Mohd Isa, H. El Kadri, D. Vigolo and K. Gkatzionis, *Micromachines (Basel)*, 2022, **13**, 2067.
49. N. K. Dewangan and J. C. Conrad, *Soft Matter*, 2019, **15**, 9368–9375.
50. B. Behkam and M. Sitti, *Appl. Phys. Lett.*, 2007; **90**, 023902.
51. R. Di Leonardo, L. Angelani, D. Dell'arciprete, G. Ruocco, V. Iebba, S. Schippa, M. P. Conte, F. Mecarini, F. De Angelis and E. Di Fabrizio*, Proc. Natl. Acad. Sci. U. A.*, 2010, 107, 9541–9545.
52. B. W. Park, J. Zhuang, O. Yasa and M. Sitti, *ACS Nano*, 2017, **11**, 8910–8923.
53. O. Felfoul, M. Mohammadi, S. Taherkhani, D. de Lanauze, Y. Zhong Xu, D. Loghin, S. Essa, S. Jancik, D. Houle, M. Lafleur, L. Gaboury, M. Tabrizian, N. Kaou, M. Atkin, T. Vuong, G. Batist, N. Beauchemin, D. Radzioch and S. Martel, *Nat. Nanotech.*, 2016, **11**, 941–947.
54. S. Suh, A. Jo, M. A. Traore, Y. Zhan, S. L. Coutermarsh-Ott, V. M. Ringel-Scaia, I. C. Allen, R. M. Davis and B. Behkam, *Adv. Sci.*, 2018, **6**, 1801309.
55. Y. S. Lee and W. Park, *Appl. Microbiol. Biotechnol.*, 2018, **102**, 3059–3070.